International Journal of Engineering Trends and Technology
ISSN: 2231-5381/ https://doi.org/10.14445/22315381/IJETT-V73I3P138

Volume 73 Issue 3, 540-553, March 2025

Original Article

Camargo's Indexive Filtering based Affine Invariant Sliced Regression for Ulcer Prediction Using Wireless Capsule Endoscopy Images

S. Bhuvaneswari[1], M. Sulthan Ibrahim[2]

[1]*Department of Computer Science, Madurai Kamaraj University, Madurai, Tamil Nadu, India.*
[2]*Department of Computer Science, Government Arts and Science College- Affiliated to Madurai Kamaraj University, Veerapandi, Theni, Tamil Nadu, India.*

[1]*Corresponding Author : bhuvanika22@gmail.com*

Received: 02 August 2024 Revised: 11 December 2024 Accepted: 27 January 2025 Published: 28 March 2025

Abstract - *An ulcer is a sore or lesion that forms in the coating of Gastro Intestinal (GI) area. The most common ulcers develop in the small intestine and stomach. In GI, ulcers tract potentially led to serious conditions like Crohn's disease and ulcerative colitis. Conventionally, detection of ulcers in the GI tract involves endoscopy techniques, which are uncomfortable for patients, and these methods may not effectively visualise the small intestine area. Therefore, WCE is the essential diagnostic task for examining the GI tract. Conventionally, ulcer detection using machines and DL methods has been developed through early detection and treatment. However, achieving accurate ulcer detection with minimal time complexity is a significant challenge. A novel technique called Camargo's Indexive Kuwahara Filtering Based Affine Invariant Sliced Regression (CIKF-AISR) is introduced to enhance accuracy and minimise time complexity. The proposed CIKF-AISR technique includes three major processes: image acquisition, preprocessing and feature extraction. First, the numbers of WCE images are collected from the dataset. After the image acquisition, preprocessing is carried out to eradicate noise and protect edges by applying an adaptive Camargo's indexive Kuwahara filtering technique for image smoothing. This helps to reduce MSE and increase PSNR. The segmentation and feature extraction process are executed to minimise the time complexity of ulcer detection. Von Neumann locality segmentation is employed to segment the image into different regions and extract the ROI with the help of Canberra distance measure between the image pixels. Then, dissimilar features are extracted using the Affine invariant saliency Sliced regression method. After extracting the features, ulcer detection is performed with higher accuracy. Experimental evaluation is carried out on several factors. The analysed results indicate that the CIKF-AISR technique achieved better performance in accuracy, PSNR, and precision and less time compared to conventional methods.*

Keywords - *Adaptive camargo's indexive kuwahara filtering technique, Affine invariant saliency, Sliced regression method, Ulcer detection, Von Neumann locality segmentation, Wireless capsule endoscopy images.*

1. Introduction

An ulcer is a lesion that forms in the lining of an organ. An ulcer occurs in various body parts, including the stomach and small intestine. Ulcer detection is vital in healthcare for timely treatment and preventing further complications such as bleeding, perforation, or infection. Ulcer detection typically involves analysing medical images, such as endoscopic images, radiographic images, dermatological images, etc, to identify lesions. Among the various images, wireless capsule endoscopy images have emerged as a valuable tool in diagnosing and managing GI disorders since they provide high-resolution images for accurate detection. Several ML and DL models have been developed to accurately detect ulcers. To enhance the visibility of WCE images, deep CNN [1] was developed. This results in improved contrast and sharper edges by amplifying the noise. However, achieving accurate ulcer detection with minimal time complexity remains a challenging issue for optimal performance. An integration of generative adversarial networks and Variational Autoencoders (VAE-GAN) for ulcer detection was developed in [2]. However, challenges in improving the accuracy of ulcer detection due to difficulties in segmenting ROI. For the classification of ulcers and erosion, the CNN model was introduced in [3]. However, the issue of image quality analysis performance remained unresolved. Endoscopic images were categorised in [4] via DL. In [5], the CNN–FFNN and the CNN–XGBoost model were developed for diagnosing gastrointestinal diseases based on endoscopy images. However, the developed hybrid models did not achieve more accuracy with minimal time. In [6], three-dimensional deep

CNN was introduced for automatic multiclass classification based on spatiotemporal information using WCE images. However, it did not explore additional investigation to fully utilise the rich information for classification. To categorise tiny bowel CE images, ML algorithms were developed [7]. However, the time complexity of detecting the ulcerated mucosa was higher. A fully automated method was designed in [8] based on deep learning for ulcer detection with higher accuracy. However, the segmentation was not accurate enough to minimise computational time. Endoscopic images are diagnosed [9] by a multi-method system. To automatically discover ulcers and erosions, multi-brand CNN was introduced in [10].

However, the accuracy of ulcer detection was not improved. A CNN model was developed in [11] for categorising Gastrointestinal tract diseases using wireless endoscopy images to speed up processes and increase efficiency. However, accurately diagnosing diseases was difficult even with a large dataset. A deep learning framework called ResNet50 was developed in [12] for detecting the severity of ulcerative colitis in capsule endoscopic images. However, it does not effectively reduce the time consumption for severity classification. Artificial intelligence models were developed in [13] to predict ulcerative colitis. However, the accuracy of ulcerative colitis prediction was not analysed. The Class-Balanced High-Resolution Network was developed in [14]. However, ulcerative colitis detection was not performed with a larger number of samples. In [15], numerous DCNNs were introduced to discover the identification of ulcerative colitis. However, huge datasets were not considered for ulcerative colitis detection. The above existing methods challenge the issue of optimal performance utilised to obtain accurate ulcer detection with reduced time complexity. Then, the accuracy of ulcer detection failed to improve the challenging issues in segmenting ROI. The model of the hybrid method failed to improve the accuracy with less time. The segmentation was not accurate and adequate to reduce computational time. The shortcoming of the proposed method using the accuracy of endoscopic diagnosis depends on the endoscopist's technical skill and clinical experience; it failed to improve the accuracy and precision. To overcome these issues, proposed Camargo's Indexive Kuwahara Filtering Based Affine Invariant Sliced Regression (CIKF-AISR) is introduced to enhance the accuracy with minimal time complexity in ulcer detection.

1.1. A Novel Contribution of the Paper

- The CIKF-AISR technique has been developed to enhance the accuracy of ulcer detection by including several processes, namely preprocessing, segmentation, and feature extraction.
- A novelty of adaptive Camargo's indexive Kuwahara filtering method is determined to improve the PSNR by using the CIKF-AISR technique for removing the noise artifacts from input endoscopy images.
- A novel Von Neumann locality segmentation method is designed to reduce the ulcer detection time via CIKF-AISR technique to extract ROI as of image depending on Canberra distance measure.
- A novelty of the affine invariant saliency Sliced regression method is performed to enhance the accuracy of ulcer detection and precision in extracting significant features. These significant features are used for accurate ulcer detection.
- Evaluate the performance of our CIKF-AISR technique using comprehensive experimentation conducted with different evaluation metrics.

1.2. Organisation of Paper

The rest of the paper is structured as follows: Section 2 reviews related works. In Section 3, the proposed CIKF-AISR technique is described in detail. Section 4 presents experimental evaluation with dataset description. Experimental results and a comprehensive quantitative analysis are discussed in section 5. In section 6, details about discuss the potential part of our proposed work. Finally, Section 7 provides the conclusion of the paper.

2. Literature Survey

Endoscopic severity grading of ulcerative colitis was detected [6] with DL. However, it could not accurately determine the more detailed automated assessment of a patient's ulcerative colitis status. Fully automated endoscopic disease activity evaluation of ulcerative colitis was developed in [17]. However, the development and validation methods were not applied to distributed disease severity datasets. The severity of ulcerative colitis was determined in [18] by Pyramid Hybrid Feature Fusion. However, time complexity was not minimised. Patients with ulcerative colitis were distinguished in [19] by the DL algorithm. Ulcerative colitis was predicted [20] by a DL-based system. However, it failed to improve its feature extraction capability to enhance the classification performance.

For accurately evaluating endoscopic images from patients, DNN for an estimate of Ulcerative Colitis was introduced in [21]. DL method distinguishes different types of inflammatory bowel disease. However, multi-task algorithms were not employed to accurately classify ulcerative colitis disease severity. Automated and quantitative calculations of universal endoscopic illness severity of ulcerative colitis were introduced in [22].

A recurrent neural network was introduced in [23] for detecting ulcerative colitis. However, the accuracy of predicting ulcerative colitis was not enhanced. Deep CNN was designed [24] to detect gastrointestinal abnormalities from endoscopic images. However, it failed to improve the accurate and time-saving abnormality detection. DCNN architecture was designed. However, DCNN did not improve the classification performance. A new pathology-sensitive deep

learning model was developed. However, it failed to effectively perform anomaly detection and classification with a greater number of videos. A multi-layer perceptron artificial neural network was designed to evaluate the diagnostic performance of ulcerative colitis. Two Convolutional Neural Network (CNN) models were developed using endoscopic images. A Deep Learning (DL) model was designed to identify Ulcerative Colitis disease patterns through three binary classification tasks.

Motivated by the above aspects, we present ulcer detection using machine and DL algorithms. Preprocessing is performed to remove the noise and also defend edges by applying an adaptive Camargo's indexive Kuwahara filtering technique for image smoothing. This helps to reduce MSE and increase PSNR. After that, the segmentation and feature extraction process are executed to reduce the time complexity of the ulcer detection.

Von Neumann locality segmentation is determined to segment the image into several regions and extract the ROI with the aid of Canberra distance measure between the image pixels. Then, dissimilar features are extracted using the Affine invariant saliency Sliced regression method. After extracting the features, ulcer detection is performed with improved accuracy.

3. Proposal Methodology

Ulcer diseases are a major health concern, affecting many people worldwide. These are characterised by lesions that develop on the inside layer of the stomach, small intestine, or other areas of the gastrointestinal area. A common symptom of ulcer diseases includes abdominal pain, indigestion, nausea, and vomiting. Detecting ulcer diseases at an early stage is crucial for effective management and treatment. Ulcer detection improved using WCE images of the GI tract. CIKF-AISR developed. It captures GI tract images to visualise an apparent view of the internal parts of the human body, unlike conventional endoscopy techniques. WCE offers a less persistent and more comfortable alternative for patients than the traditional endoscopy. The patient ingests the small capsule containing the miniature camera and transmits images because it passes through the digestive system. Conventionally, ulcer detection using machines and DL algorithms has been developed in early detection and treatment. However, achieving accurate ulcer detection with lesser time complexity faces major challenges. CIKF-AISR method was utilised to improve ulcer detection accuracy with minimal time and a higher peak-signal-to-noise ratio. Architecture diagram of proposed CIKF-AISR technique for accurate detection of Ulcer detection with WCE images demonstrated in Figure 1. The proposed ulcer recognition technique involves image acquisition, preprocessing, segmentation, and feature extraction.

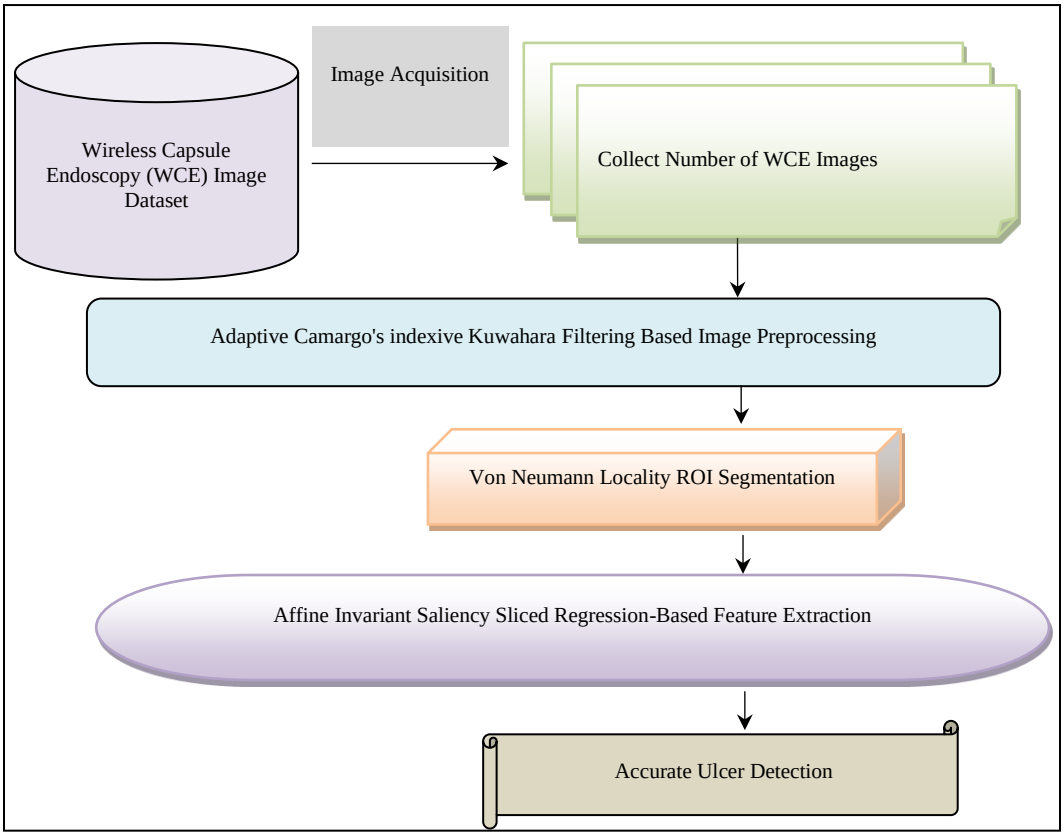

Fig. 1 Block diagram of proposed CIKF-AISR

3.1. Image Acquisition

It has the procedure of collecting the WCE image as of the Hyper-Kvasir dataset. It has a widely unconfined GI tract image dataset for ulcer detection. It is separated into four separate elements Labeled image data, unlabeled image data, segmented image data, as well as annotated video information. Amongst these parts, labeled images were employed to estimate the experimental. From the labeled images, ulcer WCE images were gathered to find the disease.

3.2. Preprocessing

Preprocessing is a fundamental step in achieving higher WCE image quality for further analysis. The proposed technique utilises Adaptive Camargo's indexive Kuwahara filtering for image denoising to improve image quality.

Camargo's indexive Kuwahara filtering reduces adaptive noise in WCE images. The proposed filter is capable of utilising smoothing on WCE images to preserve edges.

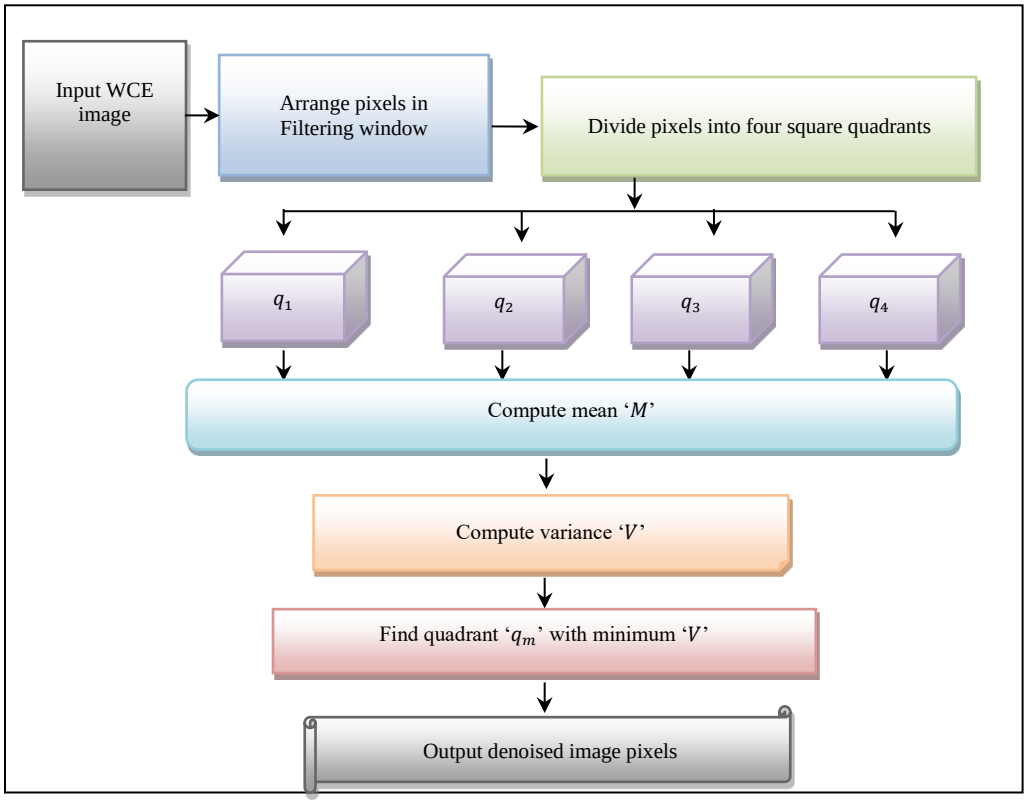

Fig. 2 Flow process of adaptive camargo's indexive kuwahara filtering technique

Figure 2 illustrates a block diagram of Adaptive Camargo's indexive Kuwahara filtering for image noise artifacts removal in a given WCE image.

Let us consider the number of inputs WCE images denoted as $EI_1, EI_2, EI_3, \ldots . EI_n$ taken from the dataset. For each input image, pixels are extracted and represented by$P_1, P_2, P_3, \ldots . P_m$. Pixels are organised by filtering window size. It measured as,

$$R = 2 * k + 1 \tag{1}$$

Where filtering window size is denoted as$R$, k denotes the radius of the filter. The four-square quadrants with size $(+1) * (k + 1)$ are used to arrange the pixels in the form of row 'i' and column 'j'where, $(1 \leq i \leq h)$ and $(1 \leq j \leq w)$. First, numbers of pixels are divided into four square quadrants, as given below,

$$q_m = P\,[(i - k, i + k) * (j - k, j + k)] \tag{2}$$

Where, q_m denotes square quadrants, input pixels of images 'P' partitioned four square quadrants such as$i - k$,$i + k$, $j - k$ and $j + k$

These four-square quadrants are expressed as follows,

$$q_1 = P(i - k, i) * (j - k, j) \tag{3}$$

$$q_2 = P(i - k, i) * (j, j + k) \tag{4}$$

$$q_3 = P(i, i + k) * (j - k, j) \tag{5}$$

$$q_4 = P(i, i + k) * (j, j + k) \tag{6}$$

The layout of a $5 * 5$ Kuwahara kernel with four square quadrants is shown below.

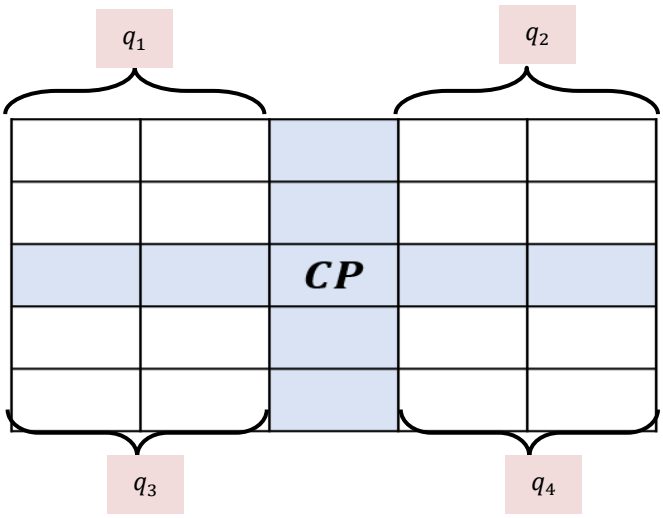

Fig. 3 Layout of a 5*5 Kuwahara filter kernel

Figure 3 illustrates the pixel arrangement or layout in $5 * 5$ Kuwahara kernel window. In ascending order, pixels are positioned. The filtering window is partitioned into four quadrants q_1, q_2, q_3 and q_4. As shown in Figure 3, CP indicates the center pixels of the kernel window. For each quadrant q, the mean (M) and deviation (M) is calculated. Then compute, the mean for each quadrant is computed as follows,

$$M(q) = \frac{1}{n\,(q)} \sum_{i=1}^{h} \sum_{j=1}^{w} Pv_{ij} \tag{7}$$

Where $M(q)$ denotes a mean of pixels, $\sum_{i=1}^{h} \sum_{j=1}^{w} Pv_{ij}$ denotes a sum of all the pixel values in the particular quadrant, the number of pixels denoted as $n\,(q)$ at a particular quadrant. Center pixels 'CP' is computed depending on the mean value follows,

$$CP = \frac{1}{4} \sum_{t=1}^{4} M_t(q) \tag{8}$$

Where, $M_t(q)$ denotes a mean of all four quadrants. After that, the deviation is computed for each quadrant based on the above estimated mean value by applying a Camargo index. Camargo's index is a qualitative method to measure the dependency between pixel values and the mean of the particular quadrant. It is formulated as below,

$$CI(q) = 1 - \sum_{i=1}^{h} \sum_{j=1}^{w} \frac{|Pv_{ij} - M(q)|}{n\,(q)} \tag{9}$$

Where $CI(q)$indicates an output Camargo's index function for a particular quadrant, Pv_{ij} denotes a pixel value in the particular quadrant,$M(q)$ indicates the mean of pixels in the particular quadrant, $n\,(q)$ indicates the number of pixels. From the analysis, the index function provides the output ranges from 0 to 1. After that, the minimum deviation among the four quadrants is identified through higher output ranges of Camargo's index function.

$$Y = \begin{cases} min\ dev\ , & CI(q) > T \\ max\ dev\ , & CI(q) < T \end{cases} \tag{10}$$

Where Y denotes a filtered output,$\min dev$denotes a minimum deviation, $\max dev$ denotes a maximum deviation T denotes a threshold, $CI(q)$indicates an output Camargo's index function. From the analysis, the pixels with minimum deviation from the mean pixels are called normal pixels.

Otherwise, the pixels with a maximum deviation from the mean are called noise pixels. The noise pixels are then removed from the filtering window through replacing the average of normal pixels within the respective quadrant. This denoising process effectively reduces MSE and enhances PSNR, resulting in enhanced image quality.

Algorithm 1: Adaptive Camargo's indexive Kuwahara filtering technique

Input: image database, Number of input WCE image $EI_1, EI_2, EI_3, \ldots . EI_n$

Output: Preprocessed images

Begin

Step 1: Collect number of input WCE image $EI_1, EI_2, EI_3, \ldots . EI_n$ from dataset
Step 2: For each input image EI_i
Step 3: Extract the number of pixels $P_1, P_2, P_3, \ldots . P_m$
Step 4: Organize the pixels in filtering window in ascending order
Step 5: Divide the image pixels into four quadrants using (3) (4) (5) (6).
Step 6: For each quadrant q
Step 7: Compute mean using (7)
Step 8: Define center pixel value 'CP' using (8)
Step 9: Compute the deviation using Camargo's index (9)
Step 10: if$(CI(q) > T)$ then
Step 11: Returns minimum deviation between the pixels and mean
Step 12: else
Step 13: Returns maximum deviation between the pixels and mean
Step 14: end if
Step 15: Select minimum deviation pixels and remove maximum deviation pixels
Step 16: Replace noisy pixels with mean value of the normal pixel
Step 17: End for
Step 18: End for
Step 19: Return **(**quality enhanced image)

End

Algorithm 1 describes the various steps involved in enhancing image quality by filtering out noise pixels. Lastly, a quality-improved image is attained with lesser MSE and higher PSNR.

3.3. Von Neumann Locality Image Segmentation

Subsequent to image preprocessing, the CIKF-AISR method carries out segmentation to partition an image into multiple segments or regions based on certain pixel intensity characteristics. The goal is to group together pixels that belong to the same object or region while separating them from other objects or backgrounds. The CIKF-AISR technique utilises the Von Neumann locality segmentation method is employed to segment the image into different regions and extract the ROI with the help of Canberra distance measure between the image pixels.

The Von Neumann locality segmentation is a concept used in image processing to define the set of spatial relationships between a set of neighboring pixels. It defines the connectivity of pixels in image processing tasks. This locality segmentation defines the notion of 4-connected pixels surrounding a central pixel.

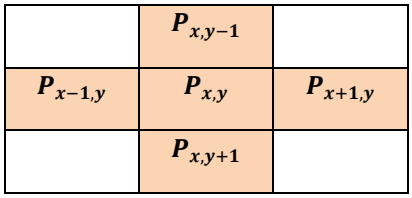

Fig. 4 Von neumann pixels connectivity

Figure 4 depicts a 4-connected neighborhood pixels method or Von Neumann pixels connectivity. First, the starting point is marked with a central pixel located in two-dimensional spaces ($P_{x,y}$). The neighborhood connectivity is measured using the Canberra distance measure between the pixels.

$$S = arg\ min\{CD(P_{x,y}, P_{NN})\} \tag{11}$$

$$P_{NN} = \begin{Bmatrix} P_{x-1,y} \\ P_{x+1,y} \\ P_{x,y-1} \\ P_{x,y+1} \end{Bmatrix} \tag{12}$$

$$CD(P_{x,y}, P_{NN}) = \frac{(P_{x,y} - P_{NN})}{|P_{x,y}| + |P_{NN}|} \tag{13}$$

Where 'S' denotes a connectivity between the pixel intensity,arg min denotes an argument of the minimum function, CD denotes a Canberra distance between the two pixels $P_{x,y}$ and P_{NN}, $P_{x,y}$ denotes a center pixel intensity, P_{NN} denotes four another pixel intensities, $|P_{x,y}|$ denotes the absolute value of center pixel intensity, $|P_{x,y}|$ denotes the absolute value of the intensity of another pixel. Therefore, the minimum distance between pixel intensities is considered adjacency or neighborhood, facilitating the connection of similar regions. This approach is utilised in image segmentation, where regions with similar pixel intensities are grouped together. Subsequently, regions of interest (ROIs), such as infected regions, are extracted for ulcer detection. This process helps minimise the time complexity of ulcer detection when considering ROIs in the image.

// Algorithm 2: Von Neumann locality Image segmentation
Input: Number of preprocessed images$EI_1, EI_2, EI_3, \ldots, EI_n$ **Output:** Segmented image
Begin **Step 1: Collect** the preprocessed images$EI_1, EI_2, EI_3, \ldots, EI_n$, **Step 2:** For every input image **Step 3:** Measure the degree of connectivity between the pixels using (11) **Step 4**: if$arg\ min\{CD(P_{x,y}, P_{NN})\}$then **Step 5**: Find Adjacent pixels **Step 6**: end if **Step 7:** end for **Step 8:** Segment the ROI from image **End**

Algorithm 2 outlines the steps involved in image segmentation to minimise the time complexity of ulcer detection. Initially, the algorithm collects a number of preprocessed images. For each image pixel, the algorithm measures the degree of connectivity between neighboring pixels using the Canberra distance metric. Subsequently, pixels with the minimum distance are connected to form the regions of interest (ROIs). Finally, the segmented images are obtained to improve the process of ulcer detection with minimal time.

3.4. Affine Invariant Saliency Sliced Regression Method-Based Feature Extraction

In order to improve ulcer detection accuracy, affine invariant saliency sliced regression performs feature extraction. Sliced inverse regression is a machine learning technique for dimensionality reduction in multivariate statistics. The dimensionality reduction is the process used to reduce the representation of an image by extracting the significant features like, shape, color and textures.

$$Z = (\omega_1{}^{\mathrm{T}} F_1,\ \omega_2{}^{\mathrm{T}} F_2, \omega_3{}^{\mathrm{T}} F_3,\ \varepsilon) \tag{14}$$

Where Z denotes a regression outcome, $\omega_1, \omega_2, \omega_3$ are projection vectors to extract the three features, namely shape, T denotes a transpose, ' F_1' indicates a shape feature, 'F_2'indicates a color feature and texture feature'F_3', the symbol ε represents the error term. It represents the difference between the observed value and the value obtained by the regression model.

Affine invariant saliency refers to a measure of the importance of image regions that remain consistent under affine transformations. To detect affine-invariant regions, an ellipse detection approach is employed for shape detection. This approach parameterises regions using three parameters, namely scale (α), axis ratio (β), and orientation (θ).

The scale parameter represents the size of the ellipse or image regions. It is defined as the average distance between the center and its boundary. Let us consider the center coordinates of object points (u_1, v_1), and the boundary coordinates of objects(u_2, v_2). The distance is computed from the center and the boundary as given below,

$$ED = \sqrt{(u_2 - u_1)^2 + (v_2 - v_1)^2} \quad (15)$$

Based on the distance measure 'ED', the closed contour is determined, which helps in identifying the shape within the image. The axis ratio parameter represents the ratio of the lengths of the major and minor axes. It is expressed as follows,

$$\beta = \frac{a}{b} \quad (16)$$

Where a denotes a major axis, b indicates a minor axis.

Orientation (θ) parameter represents the rotation angle of the ellipse relative to the x-axis.

$$\theta = \tan^{-1}\left(\frac{(u_2 - u_1)}{(v_2 - v_1)}\right) \quad (17)$$

Where, (u_1, v_1) denotes a center coordinates of points, and (u_2, v_2) denotes a boundary coordinates points.

Quantised Color Histograms are employed for the distribution of pixel intensities. The first step is to convert the image from its original color space RGB (Red, Green, Blue) to a suitable color space HSV (Hue (C_H), Saturation (C_S), Value (C_V)). The color conversion process is given below,

$$C_H = cos^{-1}\left[\frac{1}{2} * \frac{[(R-G)+(R-B)]}{\sqrt{(R-G)^2+(R-G)(G-B)}}\right] \quad (18)$$

$$C_S = 1 - 3 * \frac{1}{(R+G+B)}[argmin(R, G, B)] \quad (19)$$

$$C_V = \frac{1}{3} * [(R + G + B)] \quad (20)$$

Once the image is in the desired color space, a histogram is computed for each color channel. A histogram represents the frequency of occurrence of different color values within a specified range. If the color space is large, then it first divides into certain numbers of smaller intervals. Each of the intervals is called a bin. This process is called color quantisation. After the quantisation, the histogram is computed as follows,

$$r_i = b_1 \cup b_2 \cup b_3 \ldots\ldots \cup b_k \quad (21)$$

Where, r_i size of input color space, $b_1, b_2 \ldots b_n$ denotes a bins, $\cup$ denotes a union symbol. After that, the histogram computed for each bin is given below,

$$H(k) = count(P_i\ (b_k)) \quad (22)$$

Where, $H\ (k)$represents the histogram, i.e., the frequency of occurrence of pixels in k^{th}bin, $count(P_i\ (b_k))$ denotes counts the number of pixels in the image that have an intensity value falling within the bin b_k of the histogram. In this way, the color histogram of the image is obtained.

Texture feature provides the spatial correlation between the pixels' intensities within the ROI image.

$$Tf = \frac{1}{v_i * v_j}\sum_i \sum_j (P_i - \mu_i)(P_j - \mu_j) \quad (23)$$

Where'Tf' indicates the texture feature,P_i denotes a pixel, P_j denotes a neighboring pixel, μ_i and $\mu_j$indicates a mean of the pixels and neighboring pixels, v_i and v_j indicates a deviation of the pixels and neighboring pixels.

// **Algorithm 3: Feature extraction**
Input: segmented images ROI **Output:** extract the features
Begin **Step 1:** For each segmented image **Step 2:** Apply regression to project the feature vector using (14) **Step 3**: Extract the shape features using (15) (16) (17) **Step 4**: Convert RGB into HSV using (18) (19) (20) **Step 5:** Divide color space into bins using $r_i = b_1 \cup b_2 \cup b_3 \ldots\ldots \cup b_k$ **Step 6:** Measure color histogram (22) **Step 7:** Extract texture feature using correlation using (23) **Step 8:** end for **Step 9:** Extract significant features **End**

Algorithm 3, described above, outlines the feature extraction process for enhancing the accuracy of ulcer detection. Initially, the segmented ROI image serves as the input. Next, a regression function is utilised to project significant features from a high-dimensional space into a lower-dimensional space. Following this, affine invariant saliency is employed to extract shape features based on scale, axis ratio, and orientation. Additionally, color histograms are extracted to aid in accurate ulcer detection. Finally, texture features are extracted based on pixel correlation. The resulting features are subsequently utilised to enhance the accuracy of ulcer detection.

4. Experimental Setup

The CIKF-AISR technique and two existing methods, deep CNN [1] and VAE-GAN [2] are executed with MATLAB. In order to perform the simulation, the Hyper-Kvasir database is taken as of https://osf.io/mh9sj/. It comprises 110,079 WCE Images and 373 videos capturing anatomical landmarks, pathological results, and usual results. The dataset is divided into four separate elements. Among these parts, labeled images are used for experimental evaluation. From the labeled images, ulcer WCE images are collected, with a total of 851 available in the dataset.

For experimental purposes, 50 to 500 images are selected from the dataset. The clinical implication of our proposed CIKF-AISR technique is split into three different proposed methods: image acquisition, preprocessing and feature extraction. Initially, a number of WCE images are gathered from the dataset. After the image acquisition, preprocessing is utilised to eliminate the noise and protect edges by applying an adaptive Camargo's indexive Kuwahara filtering technique for image smoothing. This aids in minimum MSE and maximum PSNR. Subsequently, the segmentation and feature extraction process is determined to reduce the time complexity of ulcer detection. Von Neumann locality segmentation is employed to segment the image into different regions and extract the ROI with the help of Canberra distance measure between the image pixels. Then, dissimilar features are extracted using the Affine invariant saliency Sliced regression method. After extracting the features, ulcer detection is performed with better accuracy.

5. Comparative Performance Analysis

CIKF-AISR technique, along with two existing methods, deep CNN [1] VAE-GAN [2] compared. The performance analysis employs different metrics. The performance of each technique in terms of these metrics is illustrated through tables and graphical representations.

5.1. Performance Analysis of Peak Signal to Noise Ratio

The quality of the preprocessed WCE image was measured as PSNR by comparing it to the original image. SNR was determined to compute MSE among original and preprocessed WCE images.

$$PSNR = 10 * \log_{10}\left[\frac{{P_{mx}}^2}{E_{MS}}\right] \quad (24)$$

$$E_{MS} = [O_{size} - Pr_{size}]^2 \quad (25)$$

Where the peak signal-to-noise ratio is '$PSNR$', 'P_{mx}' represents maximum possible pixel value (255), E_{MS}indicates a mean square error,Pr_{size} indicates preprocessed image size, O_{size} denotes the original image size.

Table 1. PSNR

WCE Image Size (KB)	PSNR (dB)		
	CIKF-AISR	Deep CNN	VAE-GAN
228	54.15	46.54	50.06
214.7	62.11	51.22	56.08
171.3	58.58	49.04	54.15
270.4	62.11	56.08	58.58
233	60.17	52.86	57.50
235.3	63.27	55.87	59.18
244.7	57.50	51.22	54.15
191.8	64.60	50.06	55.26
266.8	60.89	53.16	57.24
267.4	63.52	55.06	58.58

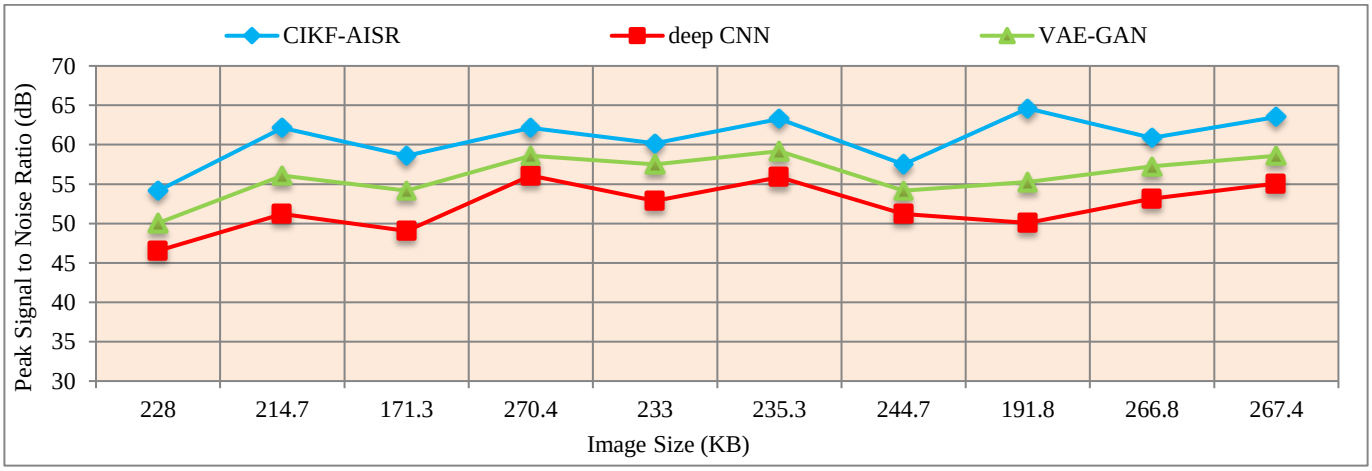

Fig. 5 Performance results of peak signal-to-noise ratio

It is expressed in Decibels (dB). Three methods, namely the CIKF-AISR technique and deep CNN [1] VAE-GAN [2], are employed in Table 1. The average of ten comparison results shows that PSNR was enhanced using the CIKF-AISR technique by 17% and 8% when compared to [1, 2]. Figure 5 depicts the performance outcomes of the peak signal-to-noise ratio with respect to different sizes of input WCE images measured in kilobytes (KB). The peak signal-to-noise ratio is measured using three methods, namely, the CIKF-AISR technique deep CNN [1] and VAE-GAN [2]. As shown in Figure 5, the CIKF-AISR technique provides improved performance in peak signal-to-noise ratio analysis. Let us consider the $228KB$ size of WCE images taken from the dataset for computing the peak signal-to-noise ratio. By applying the CIKF-AISR technique, the performance of peak signal-to-noise ratio was observed to be$54.15dB$. Likewise, the peak signal-to-noise ratio performances were observed to be $46.54dB$ and 50.06dB by applying methods [1, 2] respectively. For each method, various results were observed and compared. The average of ten comparison results shows that the peak signal-to-noise ratio was improved using the CIKF-AISR technique by 17% and 8% when compared to [1, 2], respectively. This is due to Adaptive Camargo's Indexive Kuwahara filtering technique, which enhances image quality by filtering out noise pixels from the WCE image. The image pixels are sorted into the kernel window, and Camargo's index is applied to measure the deviation between the pixels. The pixels with the maximum deviation are recognised as noise and replaced by the average of other normal pixels. These processes enhance image quality and minimise mean square error.

5.2. Performance Analysis of Ulcer Detection Accuracy

It measured the number of WCE images precisely recognised. Accuracy mathematically formulated as given below,

$$UDA = \left(\frac{TR_p+TR_n}{TR_p+TR_n+FL_p+FL_n}\right) * 100 \quad (26)$$

Where UDA indicates ulcer detection accuracy, TR_pdenotes the true positives, the true negative isTR_n, a false positive isFL_p, false negativeFL_n indicates false negative. The accuracy is measured in percentage (%).

Table 2. Ulcer detection accuracy versus the number of WCE images

Number of WCE Images	Ulcer Detection Accuracy (%)		
	CIKF-AISR	Deep CNN	VAE-GAN
50	86	78	82
100	88.6	80.36	85.32
150	91.5	82.65	86.52
200	92.12	83.6	85
250	91.96	84.8	87.23
300	91.85	85.12	88.24
350	92.65	86.54	89.12
400	91	85.12	87.54
450	90.6	83.5	85.36
500	89.36	82.56	84.52

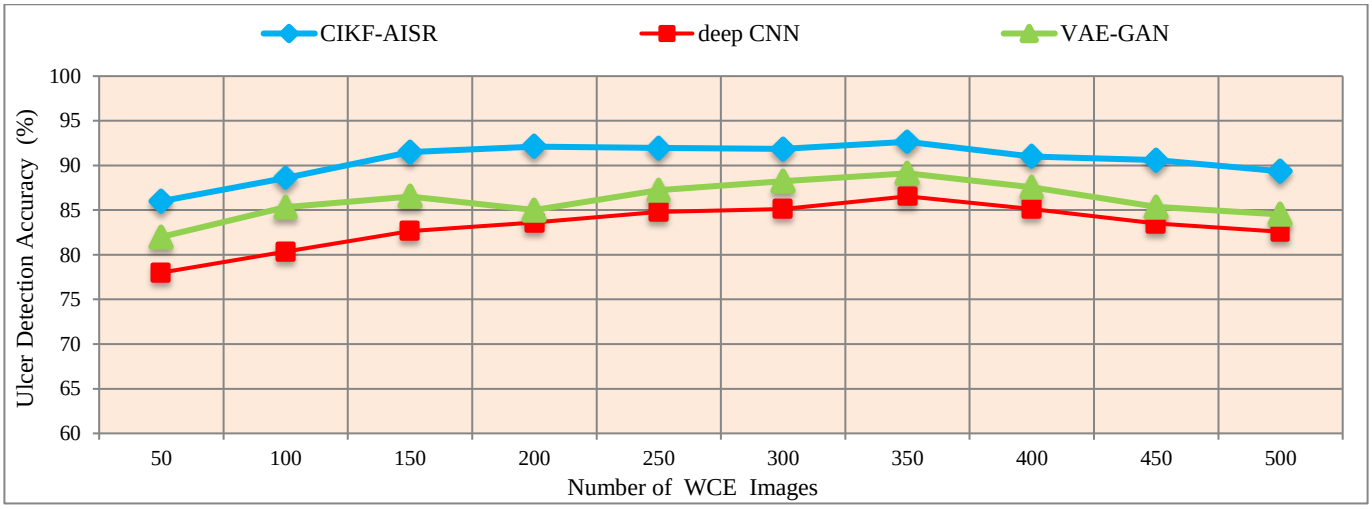

Fig. 6 Performance results of ulcer detection accuracy

Figure 6 demonstrates a performance analysis of ulcer detection accuracy versus the number of WCE images collected from the dataset, ranging from 50 to 500. The number of WCE images are taken on the horizontal axis, and the ulcer detection accuracy was observed on the vertical axis. The graphically analysed result proves that the ulcer detection accuracy of the CIKF-AISR technique was higher than existing methods [1, 2]. Let us consider the first iteration involving 50 images; the ulcer detection accuracy using the CIKF-AISR technique was 86%. Subsequently, 78% and 82% of ulcer detection accuracy were observed by applying [1] and [2], respectively. Multiple runs were carried out for each method with various numbers of input images. The performance outcomes of CIKF-AISR were compared to the results of existing methods. Overall comparison outcomes prove that the CIKF-AISR method increased accuracy by 9% compared to [1] and 5% compared to [2]. This is because the CIKF-AISR uses an Affine invariant saliency Sliced regression method to extract features like shape, color, and textures from the segmented ROI image. With the extracted features, ulcer detection is performed, resulting in enhanced accuracy.

5.3. Performance Analysis of Precision (Sensitivity)

It measures the ratio of true positive detection of ulcer disease made by the model. Precision computed by,

$$Pre = \frac{TR_p}{TR_p + FL_p} \tag{27}$$

Where Pre denotes a precision, TR_p denotes a true positive that the images are correctly detected as ulcers, FL_p indicates a false positive refers to images incorrectly detected as ulcer. Table 2 illustrates a performance analysis of precision in ulcer detection. On average, the comparison of ten results reveals that the precision performance during ulcer detection was increased by 9% compared to deep CNN [1] and by 5% compared to VAE-GAN [2]. Figure 7 illustrates a performance analysis of precision in ulcer detection versus the number of WCE images taken in the range from 50 to 500. The graph depicts the number of inputs WCE images on the 'x' axis and the precision performance observed on the 'y' axis. Among the three methods, CIKF-AISR demonstrates improved precision performance compared to the other two existing methods.

Table 3. Precision versus number of WCE images

Number of WCE Images	Precision (%)		
	CIKF-AISR	deep CNN	VAE-GAN
50	0.902	0.837	0.871
100	0.912	0.845	0.875
150	0.915	0.832	0.856
200	0.908	0.855	0.866
250	0.911	0.826	0.857
300	0.895	0.835	0.858
350	0.918	0.847	0.869
400	0.907	0.833	0.875
450	0.905	0.826	0.855
500	0.903	0.818	0.852

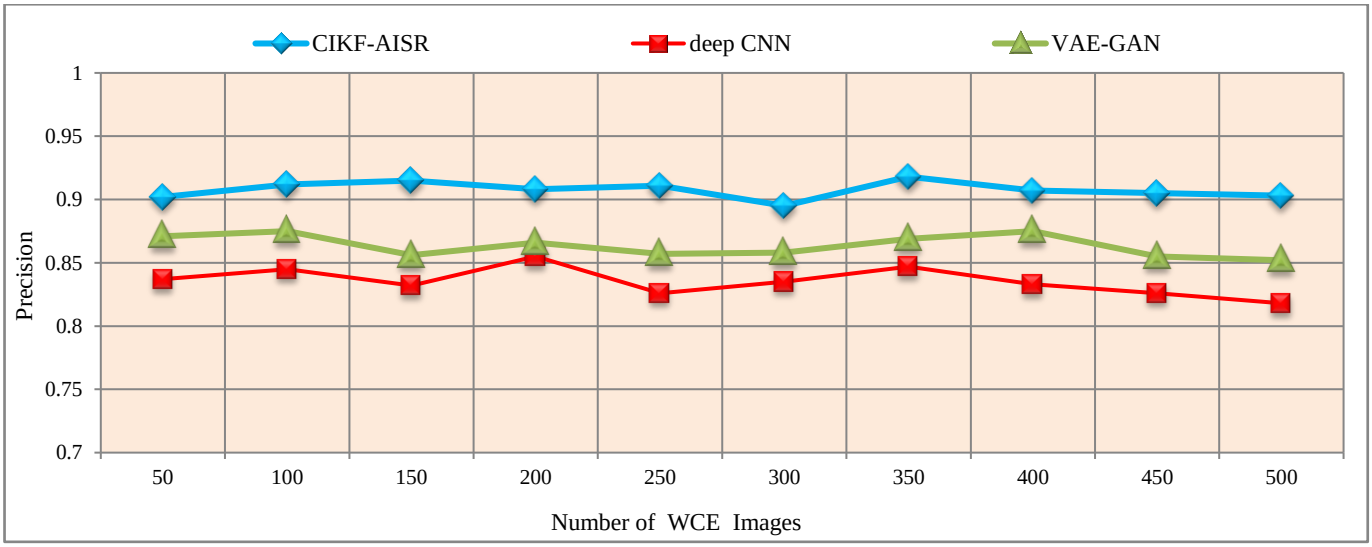

Fig. 7 Performance results of precision

This improvement is achieved due to the ut.ilisation of Affine Invariant Saliency for extracting shape features, generating color histograms based on quantisation methods, and extracting texture features based on the spatial correlation between pixels. These extracted features contribute to minimising false positives in ulcer detection and increasing the true positive rate. On average, the comparison of ten results reveals that the precision performance during ulcer detection was increased by 9% compared to deep CNN [1] and by 5% compared to VAE-GAN [2].

5.4. Performance Analysis of Ulcer Detection Time

The overall time for ulcer detection from the given input WCE images is measured as the amount of time methods taken to identify ulcers. It is mathematically calculated as follows,

$$UDT = \sum_{i=1}^{n} EI_i * Time\ \ [UD] \tag{28}$$

Where, UDT indicates the ulcer detection time, Time [UD] indicates a time for detection of a single image 'EI_i'. The overall time is estimated in milliseconds (ms).

Figure 8 illustrates the performance analysis of ulcer detection time using three methods, namely CIKF-AISR and deep CNN [1], VAE-GAN [2]. For each method, a simulation of 10 runs was performed with 500 distinct WCE images.

From the above figure, increasing the number of WCE images, the time incurred for ulcer detection was also found to be increased. However, experiments were conducted for 50 WCE images, and the time consumed for ulcer detection was 24ms using CIKF-AISR, 30.5ms using [1] and 26.5ms using [2], respectively. From this analysis, the ulcer detection time using the CIKF-AISR technique was minimised by 15% and 8% when compared to [1, 2] respectively.

The reason behind this is to perform image segmentation and ROI extraction by applying Von Neumann locality image segmentation. For each pixel in the preprocessed images, the Canberra distance metric is applied to measure the degree of connectivity between neighboring pixels. Consequently, pixels with the minimum distance are connected to form regions. Finally, the region of interest is obtained for ulcer detection, minimising time complexity.

Table 4. Ulcer detection time versus the number of WCE images

Number of WCE images	Ulcer Detection Time (ms)		
	CIKF-AISR	deep CNN	VAE-GAN
50	24	30.5	26.5
100	27.3	32.5	30.8
150	30.2	35.7	32.7
200	32.5	38.9	35.9
250	34.8	41.6	38.4
300	37.4	43.5	40.2
350	40.1	46.7	43.5
400	43.5	48.2	45.8
450	45.1	51.4	48.5
500	48.5	53.6	51.7

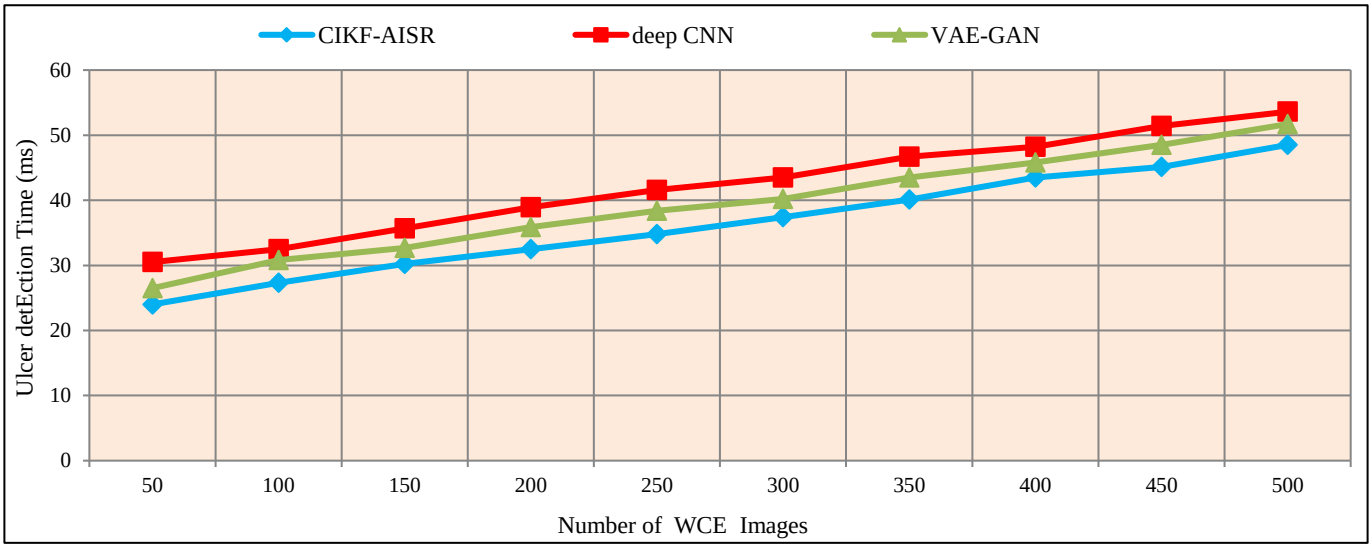

Fig. 8 Performance results of ulcer detection time

5.5. Performance Analysis of Specificity

It measures the ratio of the true positive rate and false negative rate of ulcer disease made by the model. Precision computed by,

$$Spec = \frac{T_P}{T_P + F_N} \quad (29)$$

Where '$Spec$' denotes the specificity, T_P is true positive rate (i.e., number of correctly classified positive samples by employing the corresponding method), false negative rate 'FN' (i.e., number of incorrectly classified positive samples by the respective method as negative respectively. Figure 9 describes the performance analysis of specificity in ulcer detection versus the number of WCE images taken in the range from 50 to 500. The graph depicts the number of input WCE images on the 'x' axis and the precision performance observed on the 'y' axis. Among the three methods, CIKF-AISR demonstrates improved specificity performance compared to the other two existing methods. The results of the proposed CIKF-AISR proposed method compared to specificity performance in ulcer detection were improved by 8% compared to deep CNN [1] and by 5% compared to VAE-GAN [2].

Table 5. Specificity versus the number of WCE images

Number of WCE images	Specificity (%)		
	CIKF-AISR	Deep CNN	VAE-GAN
50	0.908	0.840	0.876
100	0.917	0.849	0.880
150	0.920	0.839	0.865
200	0.910	0.863	0.870
250	0.915	0.835	0.860
300	0.905	0.840	0.863
350	0.925	0.850	0.872
400	0.913	0.839	0.877
450	0.909	0.833	0.865
500	0.915	0.825	0.867

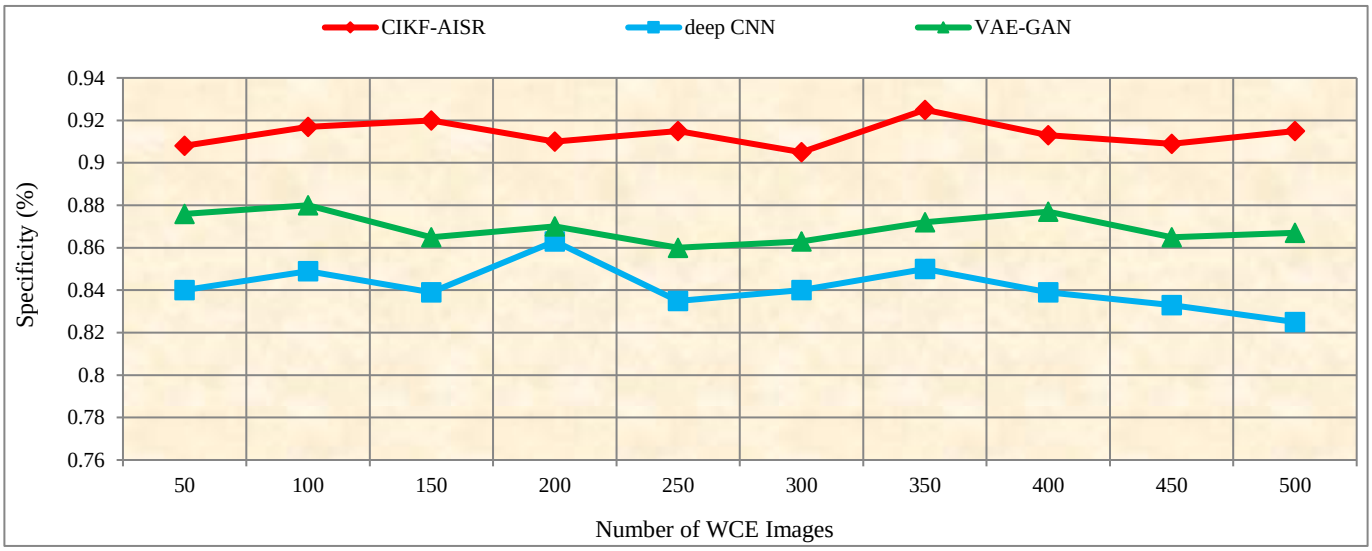

Fig. 9 Performance results of specificity

6. Discussion

This study compares the proposed CIKF-AISR technique with the existing CNN [1] and VAE-GAN [2] using the Hyper-Kvasir dataset based on different parameters, such as peak signal-to-noise ratio, ulcer detection accuracy, precision (sensitivity), and specificity and ulcer detection time are obtained by ulcer detection. Initially, image preprocessing is utilised to enhance the image quality by reducing mean square error. The segmentation of the ROI is performed to minimise ulcer detection time. The geometric methods are employed to remove different features such as shape, color, and texture features from the WCE images. With the extracted feature vector, ulcers are detected with higher accuracy. The results confirm that the proposed CIKF-AISR technique improves the ulcer detection accuracy by 7% and 13%, enhances the precision and sensitivity by 7% and 6%, and reduces the ulcer detection time by 11% compared to the existing method [1, 2] using the Hyper-Kvasir dataset.

7. Conclusion

An ulcer is a familiar irregularity introduced within the GI region. The CIKF-AISR technique has been developed with higher precision using WCE images. The CIKF-AISR technique collects input WCE images. First, image quality improved when preprocessing was performed by minimising mean square error. The segmentation of the ROI is performed to minimise ulcer detection time. Following this, geometric methods are employed to extract different features. With the extracted feature vector, ulcers are detected with higher accuracy. Comprehensive performance analysis is conducted using different metrics. Comparative results prove that the presented CIKF-AISR technique achieves higher accuracy in ulcer detection. There has also been a notable improvement in PSNR and precision. Moreover, the ulcer detection time is also minimised compared to existing methods. The discussion of limitations in our proposed CIKF-AISR method using the Hyper-Kvasir dataset is taken from https://osf.io/mh9sj/. Presently, a research group is being performed in the field of GI image and video analysis, supporting future contributions in this area. This is not limited to using the dataset for comparisons and reproducibility of experiments but also for sharing new data in the future. In future, the performance metrics of the f1 score will focus on our proposed work.

References

[1] V. Vani, and K.V. Mahendra Prashanth, "Ulcer Detection in Wireless Capsule Endoscopy Images Using Deep CNN," *Journal of King Saud University - Computer and Information Sciences*, vol. 34, no. 6, Part B, pp. 3319-3331, 2022. [CrossRef] [Google Scholar] [Publisher Link]

[2] Deepak Bajhaiya, Sujatha Narayanan Unni, and A.K. Koushik, "Deep Learning-Powered Generation of Artificial Endoscopic Images of GI Tract Ulcers," *iGIE*, vol. 2, no. 4, pp. 452-463, 2023. [CrossRef] [Google Scholar] [Publisher Link]

[3] João Afonso et al., "Development of a Convolutional Neural Network for Detection of Erosions and Ulcers with Distinct Bleeding Potential in Capsule Endoscopy," *Techniques and Innovations in Gastrointestinal Endoscopy*, vol. 23, no. 4, pp. 291-296, 2021. [CrossRef] [Google Scholar] [Publisher Link]

[4] Hsu-Heng Yen et al., "Performance Comparison of the Deep Learning and the Human Endoscopist for Bleeding Peptic Ulcer Disease," *Journal of Medical and Biological Engineering*, vol. 41, pp. 504-513, 2021. [CrossRef] [Google Scholar] [Publisher Link]

[5] Ibrahim Abdulrab Ahmed, Ebrahim Mohammed Senan, and Hamzeh Salameh Ahmad Shatnawi, "Hybrid Models for Endoscopy Image Analysis for Early Detection of Gastrointestinal Diseases Based on Fused Features," *Diagnostics*, vol. 13, no. 10, pp. 1-30, 2023. [CrossRef] [Google Scholar] [Publisher Link]

[6] Mehrdokht Bordbar et al., "Wireless Capsule Endoscopy Multiclass Classification Using Three-Dimensional Deep Convolutional Neural Network Model," *BioMedical Engineering Online*, vol. 22, no. 1, pp. 1-23, 2023. [CrossRef] [Google Scholar] [Publisher Link]

[7] Tom Kratter et al., "Deep Learning Multi-Domain Model Provides Accurate Detection and Grading of Mucosal Ulcers in Different Capsule Endoscopy Types," *Diagnostics*, vol. 12, no. 10, pp. 1-11, 2022. [CrossRef] [Google Scholar] [Publisher Link]

[8] Muhammad Attique Khan et al., "Computer-Aided Gastrointestinal Diseases Analysis from Wireless Capsule Endoscopy: A Framework of Best Features Selection," *IEEE Access*, vol. 8, pp. 132850 -132859, 2020. [CrossRef] [Google Scholar] [Publisher Link]

[9] Suliman Mohamed Fati, Ebrahim Mohammed Senan and Ahmad Taher Azar, "Hybrid and Deep Learning Approach for Early Diagnosis of Lower Gastrointestinal Diseases," *Sensors*, vol. 22, no. 11, pp. 1-31, 2022. [CrossRef] [Google Scholar] [Publisher Link]

[10] Miguel Martins et al., "Deep-Learning and Device-Assisted Enteroscopy: Automatic Panendoscopic Detection of Ulcers and Erosions," *Medicina*, vol. 59, no. 1, pp. 1-8, 2023. [CrossRef] [Google Scholar] [Publisher Link]

[11] J. Yogapriya et al., "Gastrointestinal Tract Disease Classification from Wireless Endoscopy Images Using Pretrained Deep Learning Model," *Computational and Mathematical Methods in Medicine*, vol. 2021, pp. 1-12, 2021. [CrossRef] [Google Scholar] [Publisher Link]

[12] Naoki Higuchi et al., "Automated Evaluation of Colon Capsule Endoscopic Severity of Ulcerative Colitis Using ResNet50," *PLoS One*, vol. 17, no. 6, pp. 1-13, 2022. [CrossRef] [Google Scholar] [Publisher Link]

[13] Paolo Biamonte et al., "New Technologies in Digestive Endoscopy for Ulcerative Colitis Patients," *Biomedicines*, vol. 11, no. 8, pp. 1-16, 2023. [CrossRef] [Google Scholar] [Publisher Link]

[14] Ge Wang et al., "Cb-HRnet: A Class-Balanced High-Resolution Network for the Evaluation of Endoscopic Activity in Patients with Ulcerative Colitis," *Clinical and Transaction Science*, vol. 16, no. 8, pp. 1421-1430, 2023. [CrossRef] [Google Scholar] [Publisher Link]

[15] Reed T. Sutton et al., "Artificial Intelligence Enabled Automated Diagnosis and Grading of Ulcerative Colitis Endoscopy Images," *Scientific Reports*, vol. 12, pp. 1-10, 2022. [CrossRef] [Google Scholar] [Publisher Link]

[16] Benjamin Gutierrez Becker et al., "Training and Deploying a Deep Learning Model for Endoscopic Severity Grading in Ulcerative Colitis Using Multicenter Clinical Trial Data," *Therapeutic Advances in Gastrointestinal Endoscopy*, vol. 14, pp. 1-15, 2021. [CrossRef] [Google Scholar] [Publisher Link]

[17] Heming Yao et al "Fully Automated Endoscopic Disease Activity Assessment in Ulcerative Colitis," *Gastrointestinal Endoscopy*, vol. 93, no. 3, pp. 728-736, 2021. [CrossRef] [Google Scholar] [Publisher Link]

[18] Jing Qi et al., "PHF^3 Technique: A Pyramid Hybrid Feature Fusion Framework for Severity Classification of Ulcerative Colitis Using Endoscopic Images," *Bioengineering*, vol. 9, no. 11, pp. 1-19, 2022. [CrossRef] [Google Scholar] [Publisher Link]

[19] Ji Eun Kim et al., "Deep Learning Model for Distinguishing Mayo Endoscopic Subscore 0 and 1 in Patients with Ulcerative Colitis," *Scientific Reports*, vol. 13, no. 1, pp. 1-9, 2023. [CrossRef] [Google Scholar] [Publisher Link]

[20] Jing Qi et al., "Development and Validation of a Deep Learning-Based Approach to Predict the Mayo Endoscopic Score of Ulcerative Colitis," *Therapeutic Advances in Gastroenterology*, vol. 16, pp. 1-13, 2023. [CrossRef] [Google Scholar] [Publisher Link]

[21] Kathiresh Murugesan et al., "Homomorphic Encryption, Privacy-Preserving Feature Extraction, and Decentralised Architecture for Enhancing Privacy in Voice Authentication," *International Journal of Electrical and Computer Engineering*, vol. 15, no. 2, pp. 2150-2160, 2025. [CrossRef] [Google Scholar] [Publisher Link]

[22] Sahira Vilakkumadathil, and Velumani Thiyagarajan, "Exploring Diverse Prediction Models in Intelligent Traffic Control," *Indonesian Journal of Electrical Engineering and Computer Science*, vol. 38, no. 1, pp. 393-402, 2025. [CrossRef] [Publisher Link]

[23] Ramaraj Muniappan et al., "Optimisation Techniques Applied on Image Segmentation Process by Prediction of Data Using Data Mining Techniques," *International Journal of Electrical and Computer Engineering*, vol. 15, no. 2, pp. 2161-2171, 2025. [CrossRef] [Google Scholar] [Publisher Link]

[24] Velumani Thiyagarajan et al., "Adaptive Feature Learning for Robust Pathogen Detection in Plants," *2024 4th International Conference on Sustainable Expert Systems*, Kaski, Nepal, pp. 1347-1353, 2024. [CrossRef] [Google Scholar] [Publisher Link]